Hydroxyl Radical Initiated Oxidation of *s*-Triazine: Hydrogen Abstraction Is Faster than Hydroxyl Addition

Gabriel da Silva,*,† Joseph W. Bozzelli,*,‡ and Rubik Asatryan‡

Department of Chemical and Biomolecular Engineering, The University of Melbourne, Victoria 3010, Australia, and Department of Chemistry and Environmental Science, New Jersey Institute of Technology, Newark, New Jersey 07102

Received: May 4, 2009; Revised Manuscript Received: June 5, 2009

Reaction with the hydroxyl radical (HO•) is the primary removal mechanism for organic compounds in the atmosphere, and an important process in combustion. Molecules with unsaturated carbon sites are thought to react with HO• via a rapid addition mechanism, with little or no barrier; this results in short lifetimes relative to the saturated alkanes, which undergo slower abstraction reactions. Computational chemistry and reaction rate theory are used in this study to investigate the *s*-triazine + HO• reaction. We report that HO• addition at a carbon ring site proceeds with the largest known barrier for addition to an unsaturated carbon (9.8 kcal mol^{-1} at the G3X level of theory). Abstraction of a hydrogen atom in *s*-triazine by HO•, forming the *s*-triazinyl radical + H_2O, proceeds with a barrier of only 3.3 kcal mol^{-1}, and this process dominates over HO• addition. Our results are in contrast to those for the analogous reactions in benzene, where the abstraction reaction to phenyl + H_2O is slower than the HO• addition, which forms a radical adduct that can further react with O_2 or dissociate to phenol + H•. The lifetime of *s*-triazine toward the hydroxyl radical in the troposphere is estimated at 6.4 years, potentially making it a long-lived pollutant. The aromatic *s*-triazine (1,3,5-triazine) molecule is a structural feature in herbicides such as atrazine and is a decomposition product of the common energetic material cyclotrimethylenetrinitramine (RDX). While the abstraction reaction dominates for the parent *s*-triazine, the addition mechanism may be of importance in the atmospheric degradation of substituted triazines, like atrazine, where ring H atoms are not available for abstraction. The high-barrier addition mechanism forms an activated hydroxy-triazinyl adduct which predominantly dissociates to 2-hydroxy-1,3,5-triazine (OST) + H•. This OST species is a known intermediate of RDX decomposition. Results are also presented for isomerization of the less-stable 1,3,5-triazine-*N*-oxide OST species (which may form via unimolecular pathways in the liquid-phase decomposition of RDX) to 2-hydroxy-1,3,5-triazine. A reaction mechanism is proposed for further oxidation of the *s*-triazinyl radical, where an OST isomer is also a potential product.

Introduction

The aromatic *s*-triazine (1,3,5-triazine) molecule is an important yet relatively unstudied atmospheric species (Scheme 1). Numerous common herbicides and pesticides, like atrazine, possess an *s*-triazine backbone. Triazine herbicides are known to enter the troposphere during their application (spraying) and through volatilization and soil erosion.[1] Another route to the formation of triazines in the atmosphere is through the decomposition of cyclotrimethylenetrinitramine (RDX), which contains a saturated hexahydro-*s*-triazine backbone. RDX is one of the most widely used high energy density materials, with applications as a propellant and as a high explosive. The decomposition of RDX has been extensively studied mechanistically,[2] and *s*-triazine is a known product.[3]

The destruction of *s*-triazine in the troposphere is likely to be initiated by reaction with the hydroxyl radical (HO•), which is generated photolytically. In the higher-temperature decomposition of RDX the hydroxyl radical can form via the reaction HONO + M → HO• + N•O + M (E_a = 49.5 kcal mol^{-1}),[4] where HONO is produced from RDX either via an elimination mechanism or by simple RDX dissociation to NO_2• (HONO is then formed by the NO_2• radical abstracting an H atom).[2,5] Continuation of the HONO elimination and NO_2• dissociation reactions in RDX result in *s*-triazine formation.

This study is concerned with the gas-phase reaction of *s*-triazine with HO• across temperature and pressure conditions encountered in both the atmosphere and in the explosive decomposition of energetic materials. Reaction mechanisms are proposed for HO• addition to both C and N sites in *s*-triazine, producing the $C_3N_3O_1H_3$ isomers commonly referred to as OST (oxy-*s*-triazine). The abstraction of a hydrogen atom in *s*-triazine by HO•, forming the *s*-triazinyl radical + H_2O, is also considered. We obtain thermochemical and kinetic parameters for all species and reactions in the proposed mechanisms via computational chemistry techniques. Reaction kinetics are modeled as a function of temperature and pressure according to Rice−Ramsperger−Kassel−Marcus (RRKM) theory. Isomerization of different $C_3N_3O_1H_3$ OST species is also considered.

Computational Methods

Reactants, products, intermediates, and transition states in the *s*-triazine + HO• mechanism are studied with the B3LYP/6-31G(2df,p) DFT method for molecular geometries and vibrational frequencies[6] and the G3X composite theoretical method

* To whom correspondence should be addressed. E-mail: gdasilva@unimelb.edu.au (G.d.S.); bozzelli@njit.edu (J.W.B.).
† The University of Melbourne.
‡ New Jersey Institute of Technology.

10.1021/jp904156r CCC: $40.75
Published on Web 07/02/2009

SCHEME 1: Common *s*-Triazine Molecules

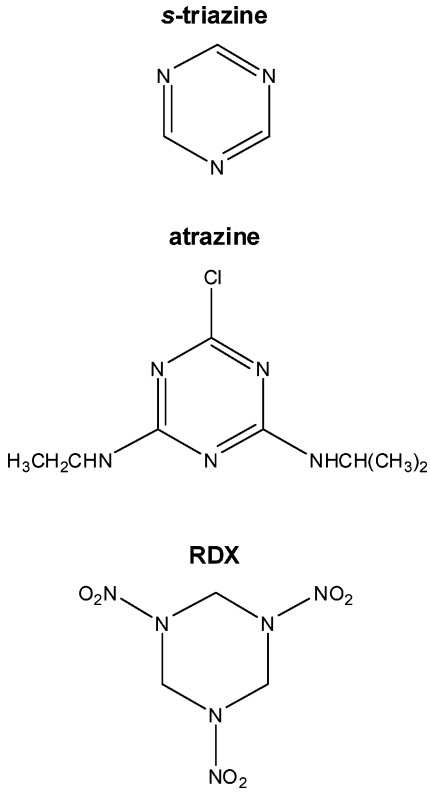

for 298 K enthalpies.[7] Calculations were performed using Gaussian 03.[8] The G3X method uses a B3LYP/6-31G(2df,p) geometry and zero point energy along with several higher-level energy calculations in which the size of the basis set decreases as the level of theory increases from Hartree−Fock through to QCISD(T). An empirical "higher-level correction" is added, accounting for the number of valence electron pairs and the number of unpaired electrons. Spin orbit corrections are also applied to single atoms. G3X theory yields a mean absolute deviation of 0.95 kcal mol^{-1} from the experimental energies of the G3/99 test set and performs even better for substituted hydrocarbons and hydrocarbon radicals (0.56 and 0.76 kcal mol^{-1}, respectively).[7] The selected theoretical methods provide accurate molecular properties at reasonable computational cost for the relatively large reaction system (7 heavy atoms) considered here.

Standard enthalpies of formation ($\Delta_f H°_{298}$) are obtained for all species at the G3X level, using atomization work reactions with reference enthalpies of 171.435 kcal mol^{-1} for C(^{3}P),[9] 112.974 kcal mol^{-1} for N(^{4}S),[10] 59.567 kcal mol^{-1} for O(^{3}P),[9] and 52.103 kcal mol^{-1} for H.[10] Thermochemical properties as a function of temperature from 300 to 3000 K are calculated according to statistical mechanical principles in the program ChemRate (version 1.5.2).[11] Low-frequency vibrational modes corresponding to internal rotation are treated as hindered rotors,[12] using B3LYP/6-31G(2df,p) internal rotor potentials. In transition states, internal rotor scans were performed with the breaking/forming bond(s) frozen.

High-pressure-limit rate constants for elementary reactions were evaluated according to canonical transition state theory in ChemRate, between 300 and 3000 K. Hydrogen abstraction reactions include Eckart quantum tunneling corrections,[13] where the characteristic barrier length (l) is obtained from eq 1 using the 0 K forward and reverse barrier heights (E_1 and E_{-1}) along with the imaginary frequency of the transition state (ν_i) and the reduced mass of H (μ).[14] Rate constants for all elementary reactions were fit to a three-parameter form of the Arrhenius equation (eq 2) in order to obtain the parameters E_a, A', and n. Apparent rate constants in the chemically activated *s*-triazine + HO$^\bullet$ reaction are evaluated as a function of temperature and pressure according to RRKM theory with time-dependent master equation (ME) analysis for pressure falloff (RRKM/ME). Decomposition of stabilized intermediates is considered via a steady-state solution of the master equation. In both cases, calculations were performed using ChemRate. An exponential-down model was used to describe collisional energy transfer, with $\langle \Delta E_{down} \rangle = 500$ cm^{-1}. Lennard-Jones collision parameters (σ and ϵ/k) are estimated from literature values for similar molecules, and all calculations feature N_2 as the bath gas. RRKM/ME rate constants are presented for the pressure range 0.01−100 atm and the temperature range 300−3000 K in the form of eq 2

SCHEME 2: Proposed Structures for the $C_3N_3O_1H_3$ (OST) Product in RDX Decomposition: (a) 1,3,5-Triazine-*N*-oxide, (b) 2-Hhydroxy-1,3,5-triazine, and (c) 1,3,5-Triazin-2(1H)-one

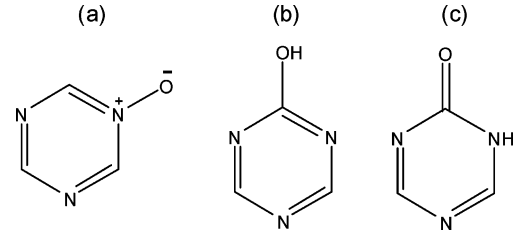

$$l = \sqrt{\frac{2(E_1^{-1/2} - E_{-1}^{-1/2})^{-2}}{\mu |\nu_i|^2}} \quad (1)$$

$$k = A' T^n \mathrm{e}^{\left(\frac{-E_a}{RT}\right)} \quad (2)$$

Results and Discussion

Energy Diagrams. Reaction mechanisms have been devised for HO$^\bullet$ addition to *s*-triazine, and for the isomerization of the OST isomers **a**, **b**, and **c** (Scheme 2). Potential energy diagrams for HO$^\bullet$ addition at N and C sites in *s*-triazine are provided in Figures 1 and 2, respectively. An energy diagram for OST isomerization is depicted in Figure 3, and the three reaction processes are discussed below. An energy diagram for the bimolecular hydrogen abstraction reaction from *s*-triazine by HO$^\bullet$ is depicted in Figure 4. For illustrative purposes, minimum energy pathways through the potential energy surfaces have been constructed according to the theory of harmonic parabolic wells.[15,16]

***N* Addition.** In Figure 1 we see that HO$^\bullet$ addition at a nitrogen atom in *s*-triazine, to the 1-hydroxy-1,3,5-triazin-4-yl radical, proceeds with endothermicity of 9.5 kcal mol^{-1} and a total barrier of almost 12 kcal mol^{-1}. The 1-hydroxy-1,3,5-triazin-4-yl adduct will carry a small degree of excess energy over the ground state radical, but the low barrier and the exothermicity for reverse reaction should be sufficient, even at relatively low temperatures, for the reverse reaction to *s*-triazine + HO$^\bullet$ to dominate.

Formation of 1,3,5-triazine-*N*-oxide (an OST isomer) requires a two-step reaction sequence: HO$^\bullet$ addition at a nitrogen atom in *s*-triazine and H atom dissociation to form H$^\bullet$ + 1,3,5-triazine-

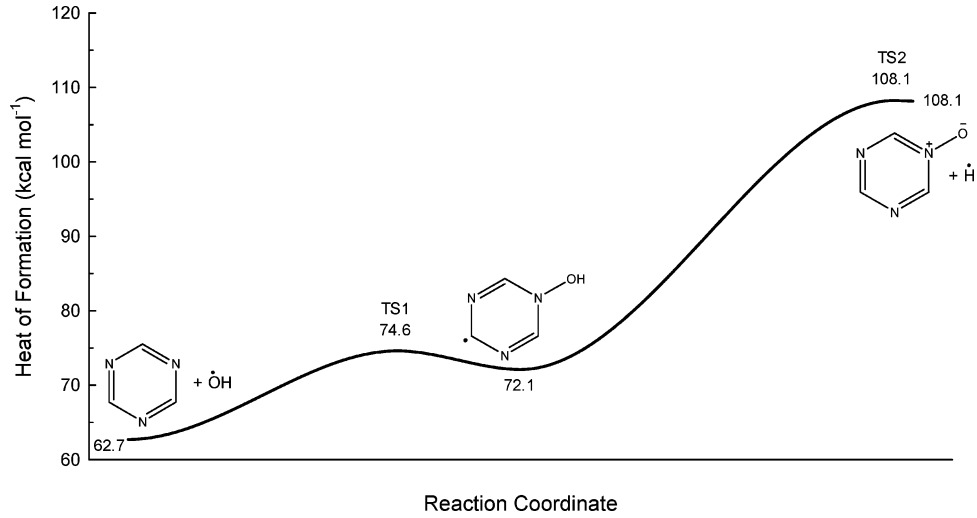

Figure 1. Energy diagram for HO$^{\bullet}$ addition to *s*-triazine at a N site. $\Delta_f H°_{298}$ in kcal mol^{-1} from G3X theory.

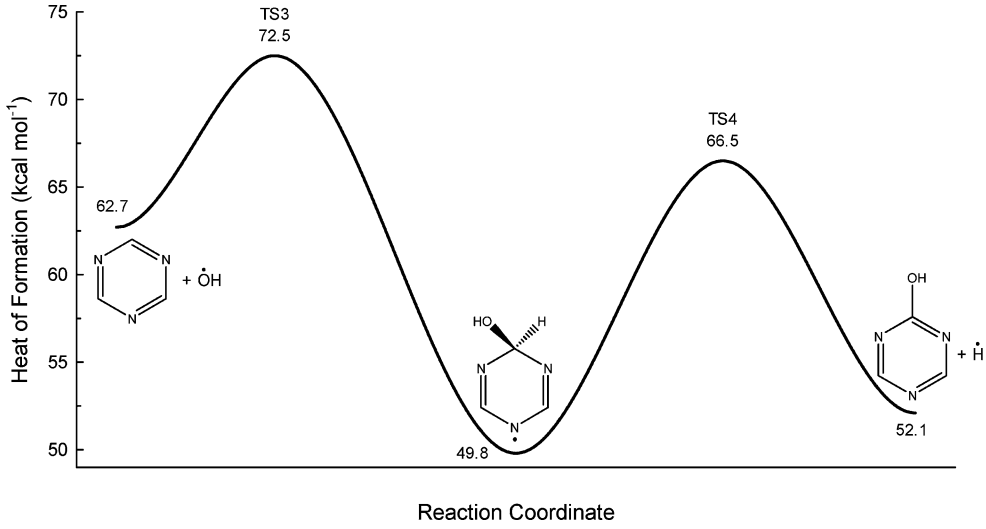

Figure 2. Energy diagram for HO$^{\bullet}$ addition to *s*-triazine at a C site. $\Delta_f H°_{298}$ in kcal mol^{-1} from G3X theory.

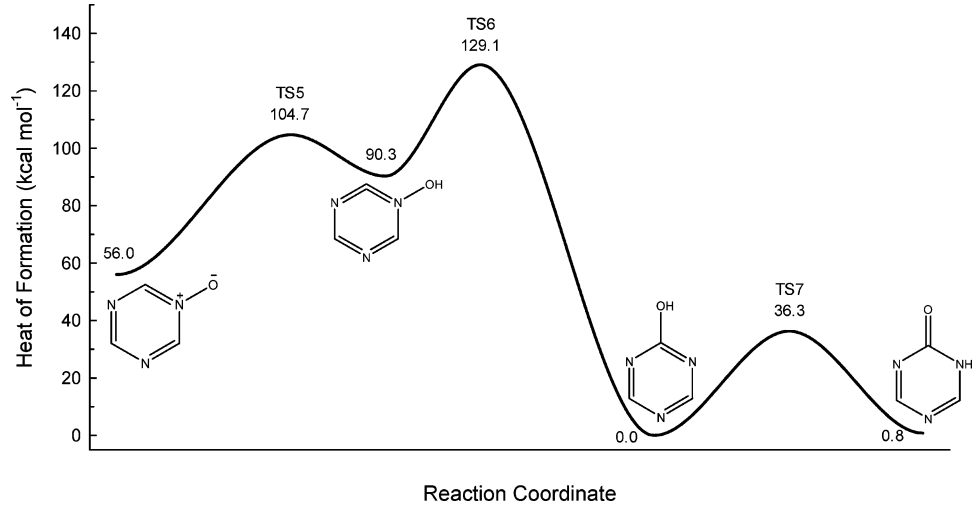

Figure 3. Energy diagram for isomerization of the different $C_3N_3O_1H_3$ (OST) species (cf. Scheme 2). $\Delta_f H°_{298}$ in kcal mol^{-1} from G3X theory.

N-oxide, which is 45.5 kcal mol^{-1} above the reactants. The initial hydroxy-1,3,5-triazin-4-yl adduct loses the relatively weak hydroxyl H atom with barrier of 36 kcal mol^{-1}, resulting in the OST isomer 1,3,5-triazine-*N*-oxide. This dissociation is essentially barrierless in the reverse direction, with a calculated activation enthalpy of only 0.09 kcal mol^{-1}. Both reaction steps in this 1,3,5-triazine-*N*-oxide formation mechanism are endothermic, with small activation barriers in the reverse direction;

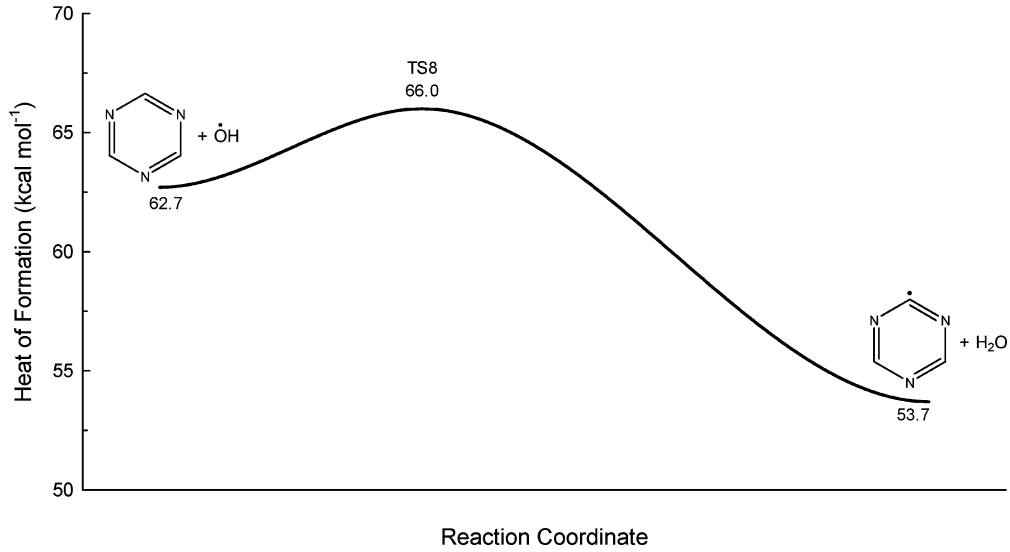

Figure 4. Energy diagram for H abstraction from *s*-triazine by HO•. $\Delta_f H°_{298}$ in kcal mol^{-1} from G3X theory.

as a result both transition states are product-like, and are located late along the reaction coordinate.

C Addition. The energy diagram for HO• addition to a carbon site in *s*-triazine is depicted in Figure 2. Addition of the HO• radical proceeds with a barrier of 9.8 kcal mol^{-1} and yields the radical intermediate 2-hydroxy-1,3,5-triazin-1-yl. This reaction is ca. 13 kcal mol^{-1} exothermic (22.7 kcal mol^{-1} below the entrance barrier), providing the hydroxytrazinyl adduct with a significant amount of excess vibrational energy. Following HO• addition, the activated adduct can cleave the weak C−H bond to provide the OST isomer 2-hydroxy-1,3,5-triazine plus H, with a barrier 6 kcal mol^{-1} below the entrance channel. In this chemically activated system the excited adduct can also undergo reverse reaction to *s*-triazine + HO• or it can be stabilized by collisions with the bath gas.

By comparison of Figures 1 and 2, we see that the C addition pathway is more energetically favorable than N addition, with forward barrier of 9.8 kcal mol^{-1} above the reactants. The OST isomer formed by the C addition mechanism is also considerably more stable than that formed by N addition, with respective enthalpies of formation of 52.1 and 108.2 kcal mol^{-1}. This provides an activated adduct with a well depth of ca. 23 kcal mol^{-1} relative to the formation barrier, with a significantly lower barrier to the formation of new products.

The reaction of HO• at a carbon site in *s*-triazine provides an interesting comparison to the analogous benzene + HO• addition reaction, which is an important process in the atmospheric destruction of benzene and other aromatic hydrocarbons. HO• addition at benzene is somewhat more exothermic than the current process (ca. 20 vs 10 kcal mol^{-1});[17] this results in a deeper well for adduct formation and no activation barrier. Dissociation of the C−H bond in the activated benzene−OH adduct also requires more energy than the similar process in *s*-triazine, further increasing the stabililty of the benzene−OH adduct relative to this *s*-triazine−OH adduct. At low to moderate temperatures the benzene + HO• reaction produces stabilized hydroxycyclohexadienyl radicals due to the relatively deep well for adduct formation; the subsequent reactions of this stabilized adduct with O_2 are important steps in the atmospheric destruction of benzene. Similar processes are expected to be important in the atmospheric degradation of *s*-triazine, although they may be less significant than OST + H• formation due to the reduced stability of the *s*-triazine−OH adduct relative to the comparable formation of phenol + H• in the benzene + HO• reaction. Comparatively, the N addition mechanism revealed above is expected to result in negligible adduct stabilization, due to the very small barrier for reverse dissociation.

To our knowledge the 9.8 kcal mol^{-1} barrier for HO• radical addition is easily the largest known for addition at an unsaturated carbon site. Such reactions typically proceed with barriers of around 1 kcal mol^{-1} or less. For example, the benzene + HO• reaction is barrierless,[18] while recent results for the furan + HO• reaction appear to indicate a modest barrier of 2.3 kcal mol^{-1} for addition at the secondary carbon atoms.[19] Addition at a carbon atom adjacent to the N atom in pyridine (C_5NH_5) requires a barrier of 4 to 7 kcal mol^{-1},[20] and the further increase in barrier height due to the presence of two neighboring N atoms in *s*-triazine appears rational. Larger barriers are known for HO• addition to nitrogen atoms, as shown here for *s*-triazine (11.9 kcal mol^{-1}) and found previously in the HN_3 + HO•[21] and N_2O + HO•[22] mechanisms (11.9 and 23.2 kcal mol^{-1}, respectively), although two of these processes are considerably endothermic and the third involves concerted addition and dissociation. The barrier height and reaction enthalpy for HO• addition at the N atom in pyridine is also similar to that determined here for *s*-triazine.[20a]

To verify this unprecedented finding of a large barrier for HO• addition to an unsaturated carbon atom, additional calculations have been performed using a variety of theoretical methods, and the results are provided in Table 1. The chosen model chemistries include additional composite methods (G3,[23] G3B3,[24] CBS-QB3[25]) as well as single-point CCSD(T) and DFT[6,26−29] calculations. From Table 1 we find that the CBS-QB3 barrier height of 4.2 kcal mol^{-1} is significantly smaller than the G3X value, although still large for an HO• addition reaction. The CBS-QB3 method uses B3LYP/6-311G(2d,d,p) structures and frequencies, along with higher-level energy corrections including a CCSD(T) energy extrapolated to the complete basis set limit. The barrier height based upon the B3LYP/6-311G(2d,d,p) enthalpies is 4.0 kcal mol^{-1}, similar to the CBS-QB3 result. The B3LYP DFT method, however, is known to chronically under-predict addition barrier heights, typically by several kcal mol^{-1}, and the B3LYP result suggests that the barrier height is actually larger than 4 kcal mol^{-1}. The G3B3 and G3 composite methods yield respective barrier heights of 7.9 and 8.4 kcal mol^{-1}, in relative agreement with G3X theory. The G3 method utilizes an MP2-optimized structure for the higher-level energy calculations, and the agreement

TABLE 1: Barrier Heights (kcal mol^{-1}) for HO$^{\bullet}$ Addition and Abstraction at a CH Site in *s*-Triazine[a]

	addition	abstraction
G3X	9.8	3.3
G3	8.4	[b]
G3B3	7.9	3.4
CBS-QB3	4.2	2.2
B3LYP	4.0	−1.7
CCSD(T)/6-311+G(2d,p)//B3LYP	9.3	6.5
BB1K/aug-cc-pVTZ//B3LYP	9.4	4.4
BMK/aug-cc-pVTZ//B3LYP	7.8	2.6
MPWB1K/aug-cc-pVTZ//B3LYP	8.8	4.2
M05−2X/aug-cc-pVTZ//B3LYP	8.2	3.4

[a] 298 K enthalpies. B3LYP structures for all DFT calculations are optimized with the 6-311G(2d,d,p) basis set. [b] Abstraction transition state could not be located at the MP2/6-31G(d) level for the G3 calculation.

between G3 and G3B3 confirms that the high barrier for HO• addition is not an artifact of the B3LYP transition state geometry. Finally, a series of single-point energy calculations were performed using the high-level CCSD(T) wave function theory method and the BB1K,[25] BMK,[27] MPWB1K,[28] and M05−2X[29] DFT methods. These DFT methods were chosen for their accuracy in reproducing barrier heights[30] and are used with the large correlation consistent augmented triple-ζ basis set aug-cc-pVTZ. The computationally intensive CCSD(T) calculations were performed with the smaller 6-311+G(2d,p) basis set. All single-point calculations feature B3LYP structures optimized with the 6-311G(2d,d,p) basis set (i.e., CBSB7) in order to test if this is the source of the discrepant CBS-QB3 result. The single-point CCSD(T) barrier height is 9.3 kcal mol^{-1}, supporting the G3X result. The DFT calculations provide barrier heights in the range of 7.8 to 9.4 kcal mol^{-1}, which are again within computational error of the G3X result but deviate more than expected from the CBS-QB3 number. For comparison, Table 1 also includes the abstraction reaction barrier height (studied in a following section), calculated using the same theoretical methods, and with this reaction we find that the CBS-QB3 result agrees with G3X and with the accurate DFT methods.

In summary, the barrier height for HO$^{\bullet}$ addition at a carbon site in *s*-triazine appears to be in the range of around 7−10 kcal mol^{-1}. The actual barrier height is likely somewhat smaller than the G3X value of 9.8 kcal mol^{-1}, however, we feel that the G3X calculations have the highest accuracy in this study.[30] We are therefore unable to justify using a different barrier height based upon our results. The CBS-QB3 method appears to fail at calculating this particular barrier height, although the reason is unclear. It can not be attributed to the use of B3LYP optimized structures (cf. G3 theory) or the 6-311G(2d,d,p) basis set (cf. single-point calculations).

Isomerization. In Figure 3 we consider interconversion of the different OST isomers arising from this study. The *N*-oxide isomer **a** undergoes intramolecular abstraction of a ring H atom, producing an even less stable *N*-hydroxy species with a barrier of 48.7 kcal mol^{-1}. The reverse reaction requires only 14.4 kcal mol^{-1}, and it is highly unlikely that this species provides a significant contribution to total $C_3N_3O_1H_3$. The hydroxyl group in this *N*-hydroxy isomer can shift from the nitrogen atom to a carbon atom in an exothermic reaction, but with barrier of around 40 kcal mol^{-1}. The more stable *C*-hydroxy OST isomer **b** will not undergo this isomerization (reverse reaction) due to the 130 kcal mol^{-1}) barrier. The 2-hydroxy-1,3,5-triazine isomer can undergo an intramolecular hydrogen shift from the hydroxy group to a ring nitrogen atom, yielding the carbonyl OST species **c**. This reaction is almost thermoneutral (1.7 kcal mol^{-1} endothermic), and both species are expected to make a significant contribution toward total $C_3N_3O_1H_3$ (OST). The reaction barrier for isomerization of the *C*-hydroxy and carbonyl isomers is 36.3 kcal mol^{-1} (34.6 kcal mol^{-1} in the reverse direction), and in a thermal system we expect this isomerization reaction to approach equilibrium.

Hydrogen Abstraction. An energy diagram for H abstraction from *s*-triazine by HO$^{\bullet}$ is presented in Figure 4. This abstraction reaction is found to proceed with a barrier of 3.3 kcal mol^{-1}, which is considerably lower than for the C addition pathway. The reaction is exothermic by 9 kcal mol^{-1}.

Further reaction of the *s*-triazinyl radical may follow a mechanism similar to the oxidation of the phenyl radical. A hypothetical mechanism for *s*-triazinyl oxidation is depicted in Scheme 3. Here, O_2 adds to the radical carbon site to form an activated peroxy radical adduct with 43.9 kcal mol^{-1} of excess energy at the G3X level. This is consistent with vinyl + O_2 (ethene C−H bond of 111 kcal mol^{-1}) and around 6 kcal mol^{-1} less than phenyl + O_2[31] (benzene C−H bond of around 113 − 114 kcal mol^{-1}).[32] The activated *s*-triazinyl-peroxy adduct could dissociate to the 1,3,5-triazin-2-oxyl radical + O, as depicted in Scheme 3.[33] In the oxidation of *s*-triazine under atmospheric conditions the peroxy adduct will be collisionally stabilized, then oxyl radical formation will occur via bimolecular reaction with NO (to $NO_2^{\bullet}$). Under low NO_x conditions the quenched peroxy radical will react with HO_2 to predominantly form a hydroperoxide molecule. Further reactions of 1,3,5-triazin-2-oxyl are somewhat uncertain, but hydrogen abstraction will form a $C_3N_3O_1H_3$ OST isomer. This provides a mechanism to OST formation through the lower-energy *s*-triazine + OH abstraction

SCHEME 3: Oxidation Mechanism for the *s*-Triazinyl Radical

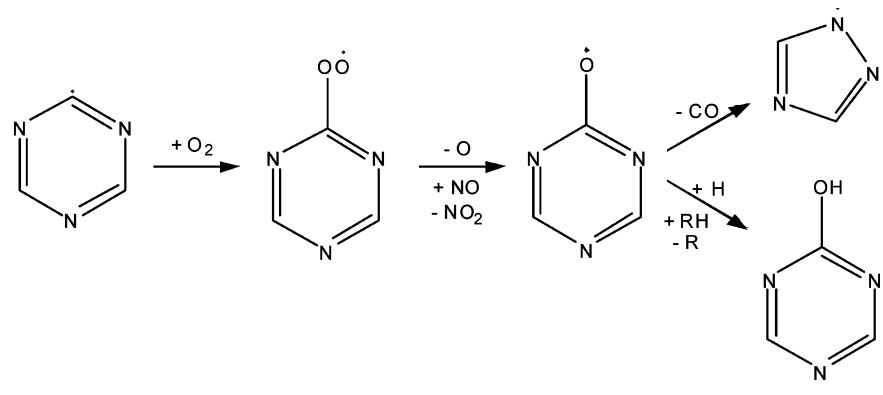

TABLE 2: Heats of Formation ($\Delta_f H°_{298}$, kcal mol^{-1}) for Studied Species in the *s*-Triazine + HO• Reaction Mechanism[a]

	$\Delta_f H°_{298}$
HO•	8.5
H_2O	−57.5
s-triazine	54.2
1-hydroxy-1,3,5-triazine-4-yl	72.1
1,3,5-triazine-*N*-oxide	56.0
2-hydroxy-1,3,5-triazine-5-yl	49.8
2-hydroxy-1,3,5-triazine	0.0
N-hydroxy-1,3,5-triazine	90.3
1,3,5-triazin-2(1H)-one	0.8
s-triazinyl	111.2
TS1	74.6
TS2	108.2
TS3	72.5
TS4	66.5
TS5	104.7
TS6	129.1
TS7	36.3
TS8	66.0

[a] Calculated at the G3X level of theory. Transition states are identified in Table 3 and Figure 5.

reaction. Alternatively, at higher temperatures, the 1,3,5-triazin-2-oxyl radical could eliminate CO to form the 1,2,4-triazol-1-yl radical, by analogy to the phenoxy radical. This triazole radical could react with peroxy radicals, or NO_2•, undergo bimolecular addition reactions with unsaturates, or abstract a hydrogen atom to form a five-membered nitrogen heterocycle (1,2,4-triazole) where the N−H bond dissociation energy is ca. 110 kcal mol^{-1} [34] (preliminary calculations show that O_2 addition at either C or N sites is unfavored in this radical). 1,2,4-Triazole is stable at temperatures up to around 600 °C,[35,36] above which it will decompose to products including HCN, NH_3, and CH_4.[35] The *s*-triazinyl radical will rapidly react with NO_2• during RDX decomposition to form an energized *s*-triazinyl radical−ONO adduct that will dissociate via cleavage of the weak RO−NO bond (∼ 43 kcal mol) to form a triazine-oxyl radical plus NO.

Structural Properties, Thermochemistry, and Rate Parameters. Table 2 lists heats of formation ($\Delta_f H°_{298}$, kcal mol^{-1}) for all species in the studied reaction paths, including transition states. Entropies ($S°_{298}$) and heat capacities as a function of temperature ($C_p(T)$) are listed in the Supporting Information. Frequencies (unscaled) and moments of inertia are provided in the Supporting Information (with structure schematics). Calculated heats of formation for HO• (8.5 kcal mol^{-1}), H_2O (−57.5 kcal mol^{-1}), and *s*-triazine (54.2 kcal mol^{-1}) agree well with experimental values (8.91,[37] −57.80,[10] and 54.0 kcal mol^{-1},[38] respectively). To our knowledge, heats of formation have not been previously reported for any of the remaining molecules, either from experiment or from first principles.

High-pressure-limit rate parameters (E_a, A', n) for the elementary reaction steps are listed in Table 3, while the transition state geometries are depicted in Figure 5. Internal C−OH and N−OH rotor potentials are provided in the Supporting Information. In *N*-hydroxy-1,3,5-triazine, 2-hydroxy-1,3,5-triazine, and TS6, internal rotation requires a barrier of larger than 11 kcal mol^{-1} and is treated as a vibrational frequency. By comparison of the two transition states for HO• addition (TS1 and TS3), we find that reaction at a nitrogen ring site (TS1) is considerably later than reaction at a carbon atom (TS3), where the X−OH bond lengths are 1.62 and 1.91 Å, respectively (compared to 1.43 and 1.40 Å in the fully formed products). This correlates with results from the potential energy surfaces developed according to the theory of intersecting harmonic wells, where the reaction coordinate for N addition is 0.69 (0 corresponds to reactants and 1 to products), while for C addition it is 0.40. The looser transition state for HO• addition at a carbon vs nitrogen site also corresponds to a higher pre-exponential factor ($A'T^n$ of 6.6×10^{-14} vs 2.3×10^{-14} cm^3 molcule^{-1} s^{-1} at 300 K). Similar results are observed for the C−H and N−H dissociation reactions in the HO• addition mechanisms. The dissociation reaction in the N addition mechanism exhibits an O−H bond length of 1.81 Å (vs 0.97 Å in the reactant) and a very-late reaction coordinate of 0.95. In the C addition mechanism we observe a C−H bond length of 1.64 Å (vs 1.12 Å in the reactant) and a balanced reaction coordinate of 0.52. In the abstraction reaction transition state the forming O−H bond is longer than the cleaving bond, consistent with an early transition state (reaction coordinate of 0.34).

Reaction Kinetics. *s-Triazine* + *HO•*. Time-dependent RRKM/ME simulations have been performed for the chemically activated *s*-triazine + HO• addition reactions, for P = 0.01 to 100 atm and T = 300 to 3000 K. Figure 6 depicts branching ratios (branching fractions) in the C addition mechanism as a function of temperature at 1 atm. Similar calculations for the N addition mechanism revealed that this process is dominated by the reverse reaction to *s*-triazine + HO•; the pathways to 1,3,5-triazine-*N*-oxide + H• and to stabilized 1-hydroxy-1,3,5-triazin-5-yl adduct were negligible under all conditions, and this reaction system is not considered further. Our RRKM calculations, at 1 atm pressure, provide the rate expressions $k = 6.40 \times 10^{-11} T^{-0.22} \exp(-14520/RT)$ cm^3 molecule^{-1} s^{-1} for the *s*-triazine + HO• → 2-hydroxy-1,3,5-triazine + H• reaction, and $k = 7.34 \times 10^{155} T^{-61.24} \exp(-32260/RT)$ cm^3 molecule^{-1} s^{-1} for the *s*-triazine + HO• → 2-hydroxy-1,3,5-triazin-5-yl stabilization reaction (results from 0.01−100 atm are in the Supporting Information). Adduct stabilization is only considered up to 600 K, after which point branching ratios for this process are negligible.

Figure 6 illustrates that stabilization of the 2-hydroxy-1,3,5-triazin-5-yl radical which results from the C addition mechanism is the dominant process at 300 K but is negligible at 500 K and above. At the lower pressures examined, typical of the stratosphere, the formation of OST + H• dominates for temperatures of 300 K and above. The lower temperatures encountered in the upper troposphere/lower stratosphere, however, result in conditions leading primarily to collision stabilization of the 2-hydroxy-1,3,5-triazin-5-yl radical. The 2-hydroxy-1,3,5-triazin-5-yl radical will undergo unimolecular decomposition to 2-hydroxy-1,3,5-triazine + H• and *s*-triazine + HO• (this is discussed below). This adduct may also undergo bimolecular reactions with species such as NO_2• to form an oxy species, and reactions such as these need to be considered in kinetic modeling of RDX decomposition. In the atmospheric oxidation of *s*-triazine the 2-hydroxy-1,3,5-triazin-5-yl radical will react predominantly with O_2. In the analogous benzene + HO• reaction, the benzene−OH adduct associates with O_2, at either an ortho or para position (meta addition results in an unstable diradical ring structure). In the 2-hydroxy-1,3,5-triazin-5-yl adduct the ortho and para sites are N atoms; O_2 addition is exothermic, and in the atmospheric oxidation of *s*-triazine the adduct formed by HO• addition will react slowly with O_2. In contrast, dissociation to OST + H• is relatively fast at even low temperatures.

TABLE 3: Rate Parameters (E_a, A', n) for Elementary Reactions Considered in the *s*-Triazine + HO• Reaction Mechanism in the Forward (f) and Reverse (r) Directions

	E_a (f)	A' (f)	n (f)	E_a (r)	A' (r)	n (r)
s-triazine + HO• → 1-hydroxy-1,3,5-triazin-4-yl (TS1)	11.62	2.45×10^{-20}	2.41	3.14	1.02×10^{13}	0.019
1-hydroxy-1,3,5-triazin-4-yl → 1,3,5-triazine-*N*-oxide + H• (TS2)	36.56	1.17×10^{12}	0.42	0.66	9.69×10^{-15}	1.25
s-triazine + HO• → 2-hydroxy-1,3,5-triazin-5-yl (TS3)	9.70	2.49×10^{-19}	2.19	23.42	8.87×10^{12}	0.11
2-hydroxy-1,3,5-triazin-5-yl → 2-hydroxy-1,3,5-triazine + H• (TS4)	16.73	6.13×10^{9}	0.94	14.55	2.54×10^{-16}	1.53
1,3,5-triazine-*N*-oxide → *N*-hydroxy-1,3,5-triazine (TS5)	49.12	1.36×10^{12}	0.49	14.76	9.17×10^{11}	0.28
N-hydroxy-1,3,5-triazine → 2-hydroxy-1,3,5-triazine (TS6)	39.54	2.65×10^{12}	0.40	129.73	8.34×10^{11}	0.88
2-hydroxy-1,3,5-triazine → 1,3,5-triazin-2(1H)-one (TS7)	36.68	2.50×10^{12}	0.37	35.85	7.72×10^{11}	0.37
s-triazine + HO• → *s*-triazinyl + H_2O (TS8)	1.94	1.54×10^{-20}	2.81	8.69	1.49×10^{-24}	3.82

[a] $k = A'T^n\exp(-E_a/RT)$. Units: E_a in kcal mol^{-1}, A' in cm^3 molecule^{-1} s^{-1} or s^{-1}. Calculated at the B3LYP/6-31G(2df,p)//G3X level of theory. High-pressure-limit rate constants, valid from 300−3000 K.

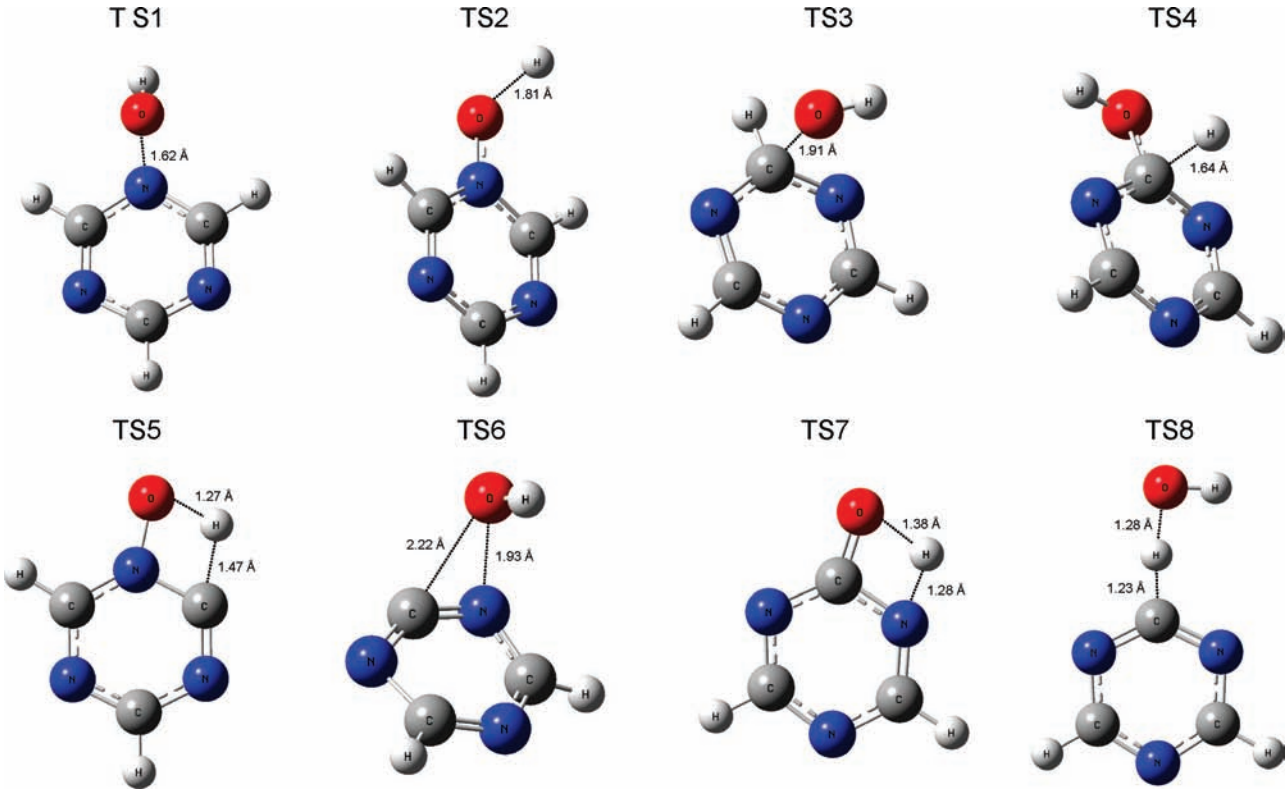

Figure 5. Molecular geometries for transition states in the *s*-triazine + HO• reaction mechanism, at the B3LYP/6-31G(2df,p) level of theory. Distances are in angstroms. Transition state numbering is identified in Table 3 and Figures 1−4.

At temperatures of 400 K and above the formation of 2-hydroxy-1,3,5-triazine (OST) + H• is the dominant process in the *s*-triazine HO• addition mechanism. OST production accounts for almost the entire reaction rate at 500 K, decreasing slightly in importance with increasing temperature as the higher barrier but entropically favored reverse reaction begins to increase in importance. Branching ratios to products at higher temperatures change little with pressure, and OST + H• are therefore expected as the dominant products of the s-triazine + HO• addition mechanism for conditions encountered in RDX decomposition.

For the *s*-triazine H abstraction reaction our transition state theory calculations provide $k = 1.54 \times 10^{-20}T^{2.81}\exp(-1940/RT)$ cm^3 molecule^{-1} s^{-1}. The abstraction rate constant incorporates an Eckart quantum tunneling correction, and tunneling increases the rate constant by around a factor of 2 at 300 K. The calculated rate expression coincides closely with recent evaluations of the benzene + HO• abstraction rate constant, where $k = 1 \times 10^{-11}\exp(-5090/RT)$[39] and $7.94 \times 10^{-11}\exp(-6309/RT)$[40] cm^3 molecule^{-1} s^{-1} (see Figure 7, where the experimental results are extrapolated over 300−3000 K).

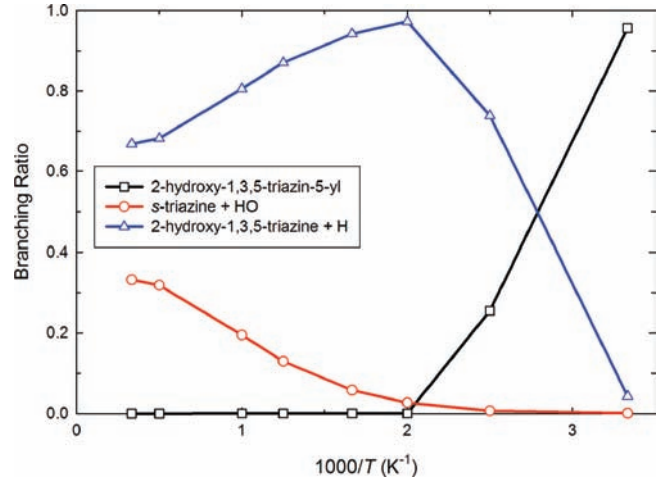

Figure 6. Branching ratios to products for the addition of HO• at a carbon ring site in *s*-triazine at 1 atm.

Abstraction of an H atom from benzene and *s*-triazine is expected to proceed at a similar rate as both molecules are

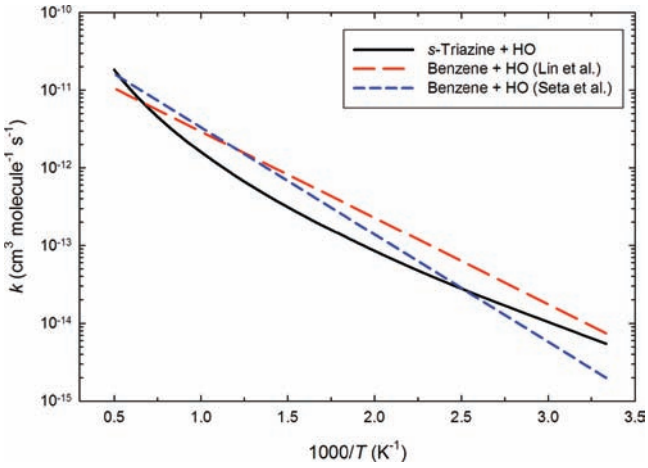

Figure 7. Rate constants for H abstraction from *s*-triazine (calculated) and benzene (experimental) by the HO• radical.

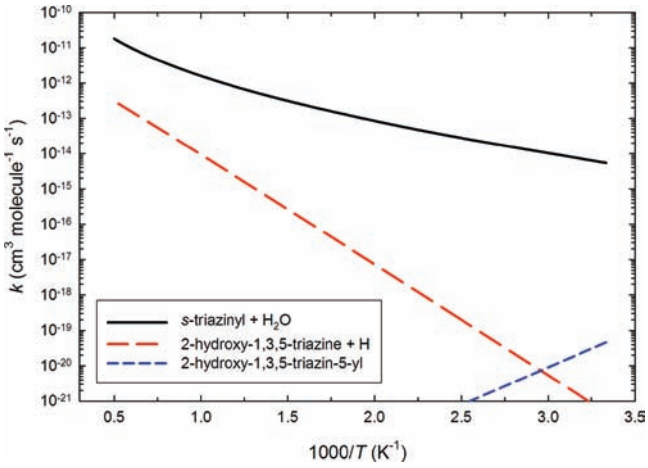

Figure 8. Calculated rate constants for formation of *s*-triazine + H_2O, 2-hydroxy-1,3,5-triazine + H•, and 2-hydroxy-1,3,5-triazin-5-yl in the *s*-triazine + HO• reaction (from rate constant fits, at 1 atm for the addition pathways).

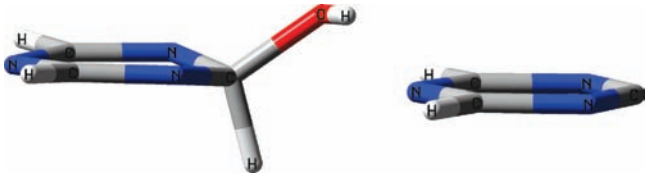

Figure 9. Tube models of the 2-hydroxy-1,3,5-triazine-5-yl and *s*-triazinyl radicals (B3LYP/6-31G(2df,p)-optimized geometries).

aromatic with similar C−H bond energies. Calculated rate constants for the *s*-triazine + HO• reaction do not agree well with an earlier reported experimental value obtained at room temperature (1.5×10^{-13} cm^3 molecule^{-1} s^{-1}),[41] which was used to deduce *s*-triazine lifetimes of 150 and 75 days, for respective "clean" and "moderately polluted" tropospheric conditions. At 300 K we obtain a rate constant of 5.48×10^{-15} cm^3 molecule^{-1} s^{-1}, which results in a much greater lifetime for *s*-triazine toward HO• in the troposphere than previously thought. By use of an average hydroxyl radical concentration of 8.7×10^5 molecule cm^{-3},[42] and by assumption that reaction with species like NO_3 and O_3 is negligible, we calculate the lifetime of *s*-triazine to be 2355 days or approximately 6.4 years (similar analysis with the Atkinson et al.[41] rate constant provides a lifetime of 89 days).

Our calculations suggest that *s*-triazine will be a long-lived atmospheric pollutant, although the uncertainty for the calculated

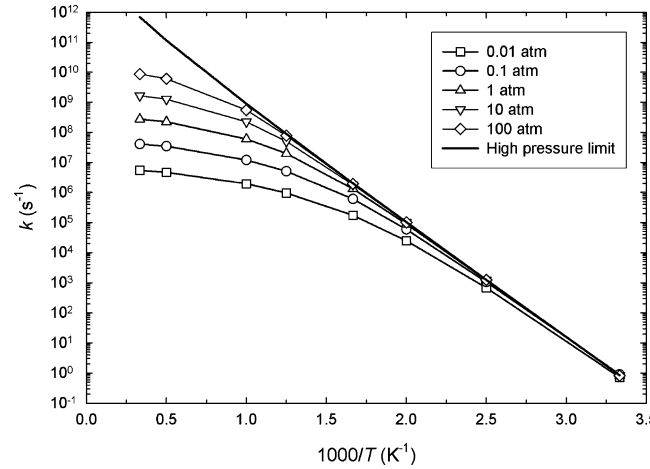

Figure 10. Unimolecular rate constants (k, s^{-1}) for the 1,3,5-triazin-5-yl → 2-hydroxy-1,3,5-triazine + H• reaction (see Figure 2) as a function of temperature and pressure.

s-triazine lifetime is relatively large. From Table 1 we see that the abstraction barrier height varies between 2.2 and 6.5 kcal mol^{-1} with a range of accurate theoretical methods with average value of 3.1 kcal mol^{-1} (whereas the G3X barrier height used here is 3.3 kcal mol^{-1}). By assumption of an error of ± 1 kcal mol^{-1} in the abstraction barrier height, the calculated *s*-triazine lifetime varies from 28 to 1.5 years. The lower value is much closer to that reported by Atkinson et al.[41] While further work is required to confirm the *s*-triazine lifetime toward atmospheric HO•, the uncertainty in barrier heights for HO• addition vs abstraction is unlikely to change the relative importance of these paths for *s*-triazine.

Figure 8 shows a comparison of calculated rate constants for formation of 2-hydroxy-1,3,5-triazine + H•, 2-hydroxy-1,3,5-triazin-5-yl, and *s*-triazinyl + H_2O from the *s*-triazine + HO• reaction (at 1 atm for the addition reactions). By comparison of calculated rate constants for the addition and abstraction reactions, we find that H abstraction to *s*-triazinyl + H_2O is the dominant reaction channel across all temperatures, being orders of magnitude greater than HO• addition at atmospheric temperatures. This provides an interesting comparison to the analogous benzene + HO• reaction, where the addition pathway is actually more rapid than H abstraction, due to the near absence of a barrier for HO• addition.

While the above results indicate that HO• addition is relatively insignificant for atmospheric *s*-triazine oxidation, this reaction may play a role in the oxidation of substituted triazines, such as atrazine, where ring H abstraction pathways are unavailable. The large barrier for HO• addition is expected to either result in large lifetimes for atrazine toward tropospheric HO•, or cause alternative reaction pathways to dominate (e.g., abstraction of nonring N−H or NHC−H hydrogens). The effect of different substituents (e.g., halides, alkyl groups, amines) on the kinetics and products of HO• addition to *s*-triazines needs further investigation.

Further work is required to better characterize the reaction rate constants and products of the *s*-triazine + HO• reaction and to understand the barrier for carbon HO• addition in *s*-triazine relative to benzene, when the C−H abstraction barriers are so similar. This difference in barrier heights to HO• addition might arise from the additional structural rearrangement that is involved in HO• addition in *s*-triazine, where the nitrogen atoms adjacent to the now tetrahedral carbon both assume a slight pyramidal structure (evident in Figure 9 and TS3 from Figure

SCHEME 4: Reaction Pathways to 1,3,5-Triazine-*N*-oxide in the Decomposition of RDX

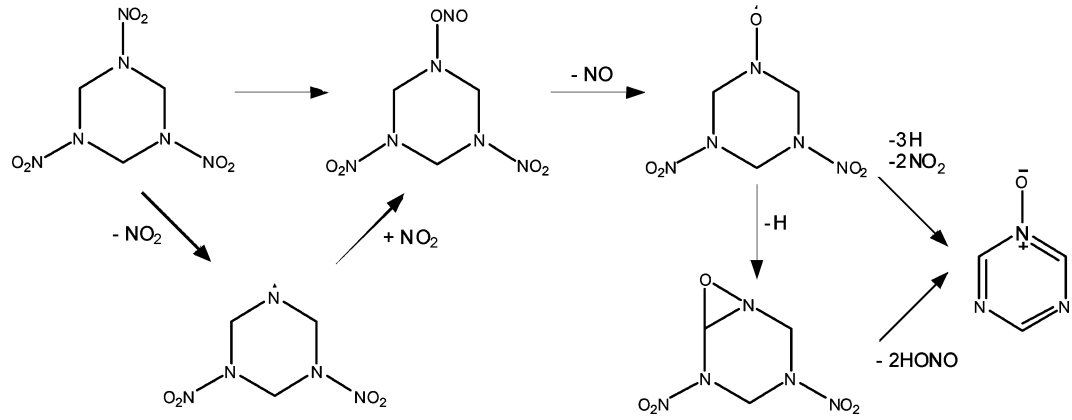

5). The average N−C(H)−N−O(OH)(H) dihedral angle in 2-hydroxy-1,3,5-triazine-5-yl is 5°, whereas all the ring dihedrals in the *s*-triazinyl radical are 0° (evident from the C_{2v} symmetry). Such a structure is caused by the presence of electron lone pairs on the nitrogen atoms, indicating loss of the delocalized aromatic structure, and this is expected to contribute to the incredibly high barrier for this addition reaction. Comparatively, a lesser degree of structural rearrangement occurs with HO• addition to benzene.[18] Such structural rearrangement is not required in the *s*-triazinyl radical (Figure 9), making it more akin to the phenyl radical.

Hydroxytriazinyl Radical Decomposition. As discussed above and shown in Figure 6, a minor pathway in the *s*-triazine + HO• reaction is stabilization of the intermediate 2-hydroxy-1,3,5-triazin-5-yl radical at low to moderate temperatures (<500 K). The further reactions of this radical (both unimolecular and bimolecular) need to be considered. Decomposition of the 2-hydroxy-1,3,5-triazin-5-yl radical to 2-hydroxy-1,3,5-triazine + H• and to *s*-triazine + HO• is studied here, as a function of temperature and pressure, from a steady-state solution of the master equation. Reaction proceeds quantitatively to 2-hydroxy-1,3,5-triazine + H•, with negligible formation of *s*-triazine + HO• across all temperature and pressure conditions (branching ratios of no greater than 0.0002). Rate constants for the 2-hydroxy-1,3,5-triazin-5-yl → 2-hydroxy-1,3,5-triazine + H• reaction are plotted in Figure 10 as a function of temperature and pressure, along with the high-pressure-limit value from Table 3. Fitted rate parameters are provided in the Supporting Information. We observe that falloff becomes significant for high-temperature low-pressure conditions, as would be expected. At atmospheric pressure, falloff is important at temperatures of around 800 K and greater. Our results reveal that decomposition of the 2-hydroxy-1,3,5-triazin-5-yl radical is rapid at even low temperatures, with a half-life of only 0.8 s at 300 K and 1 atm. It is therefore unlikely that bimolecular reactions of the 2-hydroxy-1,3,5-triazin-5-yl radical will be of major significance, even in the atmospheric oxidation of *s*-triazine.

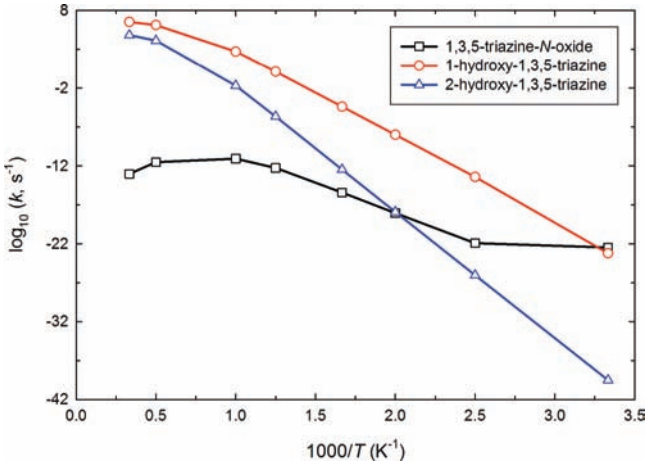

Figure 11. Rate constants (k, s^{-1}) for the isomerization of 1,3,5-triazine-*N*-oxide at 1 atm.

OST Isomerization. While the formation of 1,3,5-triazine-*N*-oxide via HO• addition to *s*-triazine is unimportant, this species may form via other routes in RDX decomposition. Scheme 4 shows a pathway to 1,3,5-triazine-*N*-oxide that is currently being considered in our research group. In this scheme one of the NO_2 functionalities in RDX undergoes a nitro−nitrite rearrangement, forming dinitro-*s*-triazine nitrite (this process could feasibly take place at any stage in RDX decomposition, following loss of NO, HONO, or NO_2•). The thermochemistry of these nitro−nitrite rearrangements has been recently studied in nitroalkanes, where the nitrite isomers are only marginally less stable (ca. 2 kcal mol^{-1}) than the nitro ones.[43] An alternative route to dinitro-*s*-triazine nitrite formation, also depicted in Scheme 4, is via N−NO_2 dissociation in RDX, followed by end-on addition of another nitro radical; in such reactions dinitro-*s*-triazine nitrite would be formed with considerable excess energy, available for further chemical activation reactions. Following the formation of dinitro-*s*-triazine nitrite, RO−NO bond dissociation may occur, providing a nitroxyl radical (dinitro-*s*-triazine-*N*-oxyl). In the alkyl nitrites, RO−NO bond dissociation energies (BDEs) are on the order of 42 kcal mol^{-1},[43] which is almost 20 kcal mol^{-1} below that of C−ONO dissociation. Subsequent loss of a weak hydrogen (by abstraction or C−H bond scission) in the nitroxyl radical followed by consecutive HONO elimination reactions, or N−NO_2 bond dissociations followed by H abstractions or scissions, finally result in 1,3,5-triazine-*N*-oxide. Two such pathways are depicted in Scheme 4, although others would be available. 1,3,5-Triazine-*N*-oxide is expected to rearrange to the more-stable *C*-hydroxy and carbonyl OST isomers according to the reactions proposed in Figure 4.

We have investigated the isomerization kinetics of 1,3,5-triazine-*N*-oxide from RRKM calculations. We treated the initial rearrangement of 1,3,5-triazine-*N*-oxide to *N*-hydroxy-1,3,5-triazine as producing a chemically activated species that is then able to undergo reverse reaction to 1,3,5-triazine-*N*-oxide, forward reaction to 2-hydroxy-1,3,5-triazine, or stabilization (*N*-hydroxy-1,3,5-triazine). The reverse reaction of 2-hydroxy-1,3,5-triazine to

N-hydroxy-1,3,5-triazine is not considered due to the high barrier for reaction. Similarly, the imine-amide rearrangement of 2-hydroxy-1,3,5-triazine to 1,3,5-triazin-2(1H)-one is neglected, as this process (in both the forward and reverse directions) should be rapid at any temperature where the higher-energy 1,3,5-triazine-*N*-oxide to 2-hydroxy-1,3,5-triazine rearrangement takes place. Figure 11 shows rate constants for 1,3,5-triazine-*N*-oxide isomerization at 1 atm from RRKM/ME simulations. The most rapid process is reverse reaction of the activated molecule to 1,3,5-triazine-*N*-oxide (i.e., no net reaction). At lower temperatures a significant fraction of the activated *N*-hydroxy-1,3,5-triazine population becomes stabilized by bath gas collisions, although at higher temperatures this is the least significant pathway due principally to the small barrier for reverse reaction. Forward reaction to 2-hydroxy-1,3,5-triazine is slow at lower temperatures, because of the relatively large overall energy barrier (ca. 73 kcal mol^{-1}) but increases in importance with increasing temperature. Apparent rate parameters have been fit to the two reactions to new products at 1 atm: for the 1,3,5-triazine-*N*-oxide → 2-hydroxy-1,3,5-triazine reaction we find k (s^{-1}) = 4.25 × 10$^{47}T^{-10.45}$exp(−42560/T) and for the 1,3,5-triazine-*N*-oxide → *N*-hydroxy-1,3,5-triazine reaction we obtain the relatively crude approximation k (s^{-1}) = 1.10 × 10$^{23}T^{-9.46}$ exp(−16530/T). For the reaction to *N*-hydroxy-1,3,5-triazine, a two-parameter Arrhenius fit up to 1000 K (before falloff becomes significant) we obtain A = 4.5 × 10^{14} s^{-1} and E_a = 74.42 kcal mol^{-1}, where the activation energy is relatively similar to the overall activation enthalpy (298 K) of 73.1 kcal mol^{-1}.

Conclusions

We have studied the kinetics and mechanism of the *s*-triazine + HO$^\bullet$ reaction, using computational chemistry and RRKM reaction rate theory. Addition of HO$^\bullet$ at C and N ring sites in *s*-triazine is shown to have very high barriers compared to addition at other unsaturated sites; the C addition mechanism is found to be the more energetically favorable. This reaction proceeds with a barrier of around 9 kcal mol^{-1} to the 2-hydroxy-1,3,5-triazin-5-yl adduct, which dissociates to 2-hydroxy-1,3,5-triazine + H$^\bullet$ at temperatures of around 500 K and above. Hydrogen abstraction from *s*-triazine by HO$^\bullet$, producing the *s*-triazinyl radical + H_2O, requires a barrier of around 4 kcal mol^{-1} and dominates over the C addition mechanism. This is in contrast to the analogous benzene + HO$^\bullet$ reaction, where barrierless HO$^\bullet$ addition is more rapid than H abstraction. The lifetime for reaction of *s*-triazine with atmospheric HO$^\bullet$ is calculated as 6.4 years, in considerable disagreement with a previous experimental value of 150 days; this highlights the need for further work on atmospheric *s*-triazine destruction mechanisms.

Acknowledgment. The authors acknowledge partial funding for this study from the U.S. Army Research office under the direction of Dr. Robert Shaw. J.W.B. acknowledges discussions with William Anderson and Richard Behrens.

Supporting Information Available: Internal rotor potentials, entropies and heat capacities, vibrational frequencies, moments of inertia, and symmetry point groups, apparent RRKM rate constant expressions in the *s*-triazine + HO$^\bullet$ C addition mechanism.This material is available free of charge via the Internet at http://pubs.acs.org.

References and Notes

(1) (a) Wu, T. L. *Water, Air, Soil Poll.* **1981**, *15*, 173. (b) Sauret, N.; Millet, M.; Herckes, P.; Mirabel, P.; Wortham, H. *Environ. Pollut.* **2000**, *110*, 243. (c) Zhang, Q.; Crittenden, J. C.; Shonnard, D.; Mihelcic, J. R. *Chemosphere* **2003**, *50*, 1377. (d) Scheyer, A.; Morville, S.; Mirabel, P.; Millet, M. *Atmos. Environ.* **2007**, *41*, 3604.

(2) (a) Behrens, R., Jr.; Bulusu, S. *J. Phys. Chem.* **1992**, *96*, 8877. (b) Behrens, R., Jr.; Bulusu, S. *J. Phys. Chem.* **1992**, *96*, 8891. (c) Wu, C. J.; Fried, L. E. *J. Phys. Chem. A* **1997**, *101*, 8675. (d) Chakraborty, D.; Muller, R. P.; Dasgupta, S.; Goddard, W. A., III. *J. Phys. Chem. A* **2000**, *104*, 2261. (e) Chakraborty, D.; Muller, R. P.; Dasgupta, S.; Goddard, W. A., III. *J. Comput.-Aid. Mater. Des.* **2001**, *8*, 203. (f) Irikura, K. K.; Johnson, R. D., III. *J. Phys. Chem. A* **2006**, *110*, 13974.

(3) Maharrey, S.; Behrens, R., Jr. *J. Phys. Chem. A* **2005**, *109*, 11236.

(4) Asatryan, R.; Bozzelli, J. W.; Simmie, J. M. *Int. J. Chem. Kinet.* **2007**, *39*, 378.

(5) (a) Velardez, G. F.; Alavi, S.; Thompson, D. L. *J. Chem. Phys.* **2005**, *123*, 074313. (b) Johnson, M. A.; Truong, T. N. *J. Phys. Chem. A* **1999**, *103*, 8840. (c) Zhang, Y.-X.; Bauer, S. H. *Int. J. Chem. Kin.* **1999**, *31*, 655. (d) Nigenda, S. E.; McMillen, D. F.; Golden, D. M. *J. Phys. Chem.* **1989**, *93*, 1124.

(6) (a) Becke, A. D. *J. Chem. Phys.* **1993**, *98*, 5648. (b) Lee, C.; Yang, W.; Parr, R. G. *Phys. Rev. B.* **1988**, *37*, 785.

(7) Curtiss, L. A.; Redfern, P. C.; Raghavachari, K.; Pople, J. A. *J. Chem. Phys.* **2001**, *114*, 108.

(8) Frisch, M. J.; Trucks, G. W.; Schlegel, H. B.; Scuseria, G. E.; Robb, M. A.; Cheeseman, J. R.; Montgomery, J. A.; Jr., Vreven, T.; Kudin, K. N.; Burant, J. C.; Millam, J. M.; Iyengar, S. S.; Tomasi, J.; Barone, V.; Mennucci, B.; Cossi, M.; Scalmani, G.; Rega, N.; Petersson, G. A.; Nakatsuji, H.; Hada, M.; Ehara, M.; Toyota, K.; Fukuda, R.; Hasegawa, J.; Ishida, M.; Nakajima, T.; Honda, Y.; Kitao, O.; Nakai, H.; Klene, M.; Li, X.; Knox, J. E.; Hratchian, H. P.; Cross, J. B.; Adamo, C.; Jaramillo, J.; Gomperts, R.; Stratmann, R. E.; Yazyev, O.; Austin, A. J.; Cammi, R.; Pomelli, C.; Ochterski, J. W.; Ayala, P. Y.; Morokuma, K.; Voth, G. A.; Salvador, P.; Dannenberg, J. J.; Zakrzewski, V. G.; Dapprich, S.; Daniels, A. D.; Strain, M. C.; Farkas, O.; Malick, D. K.; Rabuck, A. D.; Raghavachari, K.; Foresman, J. B.; Ortiz, J. V.; Cui, Q.; Baboul, A. G.; Clifford, S.; Cioslowski, J.; Stefanov, B. B.; Liu, G.; Liashenko, A.; Piskorz, P.; Komaromi, I.; Martin, R. L.; Fox, D. J.; Keith, T.; Al-Laham, M. A.; Peng, C. Y.; Nanayakkara, A.; Challacombe, M.; Gill, P. M. W.; Johnson, B.; Chen, W.; Wong, M. W.; Gonzalez, C.; and Pople, J. A. *Gaussian 03*, revision D.01; Gaussian, Inc., Wallingford CT, 2004.

(9) Ruscic, B.; Pinzon, R. E.; Morton, M. L.; von Laszevski, G.; Bittner, S. J.; Nijsure, S. G.; Amin, K. A.; Minkoff, M.; Wagner, A. F. *J. Phys. Chem. A* **2004**, *108*, 9979.

(10) Chase, M. W., Jr. *J. Phys. Chem. Ref. Data, Monograph* **1998**, *9*, 1.

(11) Mokrushin, V.; Bedanov, V.; Tsang, W.; Zachariah, M.; Knyazev, V. *ChemRate*, version 1.5.2; National Institute of Standards and Testing: Gaithersburg, MD, 2006.

(12) (a) Pitzer, K. S. *J. Chem. Phys.* **1946**, *14*, 239. (b) Pitzer, K. S.; Gwinn, W. D. *J. Chem. Phys.* **1942**, *10*, 428.

(13) Eckart, C. *Phys. Rev.* **1930**, *35*, 1303.

(14) (a) Tokmakov, I. V.; Park, J.; Gheyas, S.; Lin, M. C. *J. Phys. Chem. A.* **1999**, *103*, 3636. (b) da Silva, G. *Chem. Phys. Lett.* **2009**, *474*, 13. (c) da Silva, G.; Cole, J. A.; Bozzelli, J. W. *J. Phys. Chem. A* **2009**, *113*, 6111.

(15) Kurz, J. L. *Chem. Phys. Lett.* **1978**, *57*, 243.

(16) da Silva, G.; Kennedy, E. M.; Dlugogorski, B. Z. *J. Phys. Org. Chem.* **2007**, *20*, 167.

(17) Lay, T. H.; Bozzelli, J. W.; Seinfeld, J. H. *J. Phys. Chem.* **1996**, *100*, 6543.

(18) Chen, C.-C.; Bozzelli, J. W.; Farrell, J. T. *J. Phys. Chem. A* **2004**, *108*, 4632.

(19) Mousavipour, S. H.; Ramazani, S.; Shahkolahi, Z. *J. Phys. Chem. A* **2009**, *113*, 2838.

(20) (a) Vivekananda, S.; Wolken, J. K.; Turecek, F. *J. Phys. Chem. A* **2001**, *105*, 9130. (b) Barckholtz, C.; Barckholtz, T. A.; Hadad, C. M. *J. Phys. Chem. A* **2001**, *105*, 140. (c) Yeung, L. Y.; Elrod, M. J. *J. Phys. Chem. A* **2003**, *107*, 4470.

(21) Li, S.; Zhang, Q.; Wang, W. *Chem. Phys. Lett.* **2006**, *428*, 262.

(22) Mebel, A. M.; Lin, M. C.; Morokuma, K.; Melius, C. F. *Int. J. Chem. Kinet.* **1996**, *28*, 693.

(23) Curtiss, L. A.; Raghavachari, K.; Redfern, P. C. *J. Chem. Phys.* **1998**, *109*, 7764.

(24) Baboul, A. G.; Curtiss, L. A.; Redfern, P. C.; Raghavachari, K. *J. Chem. Phys.* **1999**, *110*, 7650.

(25) Montgomery, J. A., Jr.; Frisch, M. J.; Ochterski, J. W.; Petersson, G. A. *J. Chem. Phys.* **1999**, *110*, 2822.

(26) Zhao, Y.; Lynch, B. J.; Truhlar, D. G. *J. Phys. Chem. A* **2004**, *108*, 2715.

(27) Boese, A. D.; Martin, J. M. L. *J. Chem. Phys.* **2004**, *121*, 3405.

(28) Zhao, Y.; Truhlar, D. G. *J. Phys. Chem. A* **2004**, *108*, 6908.

(29) Zhao, Y.; Schultz, N. E.; Truhlar, D. G. *J. Chem. Theory Comput.* **2006**, *2*, 364.

(30) Zheng, J.; Zhao, Y.; Truhlar, D. G. *J. Chem. Theory Comput.* **2009**, *5*, 808.

(31) (a) Carpenter, B. K. *J. Am. Chem. Soc.* **1993**, *115*, 9806. (b) Yu, T.; Lin, M. C. *J. Am. Chem. Soc.* **1994**, *116*, 9571. (c) Mebel, A. M.; Lin, M. C. *J. Am. Chem. Soc.* **1994**, *116*, 9577. (d) Barckholtz, C.; Fadden, M. J.; Hadad, C. M. *J. Phys. Chem. A* **1999**, *103*, 8108. (e) Tokmakov, I. V.; Kim, G.-S.; Kislov, V. V.; Mebel, A. M.; Lin, M. C. *J. Phys. Chem. A* **2005**, *109*, 6114. (f) da Silva, G.; Chen, C.-C.; Bozzelli, J. W. *J. Phys. Chem. A* **2007**, *111*, 8663. (g) Sebbar, N.; Bozzelli, J. W.; Bockhorn, H. *Int. J. Chem. Kinet.* **2008**, *32*, 583.

(32) da Silva, G.; Bozzelli, J. W. *J. Phys. Chem. A* **2009**, *113,* 6979.

(33) (a) Gu, X.; Zhang, F.; Kaiser, R. I. *Chem. Phys. Lett.* **2007**, *448*, 7. (b) da Silva, G.; Bozzelli, J. W. *J. Phys. Chem. A* **2008**, *112*, 3566.

(34) da Silva, G.; Moore, E. E.; Bozzelli, J. W. *J. Phys. Chem. A* **2006**, *110*, 13979.

(35) Kumasaki, M.; Wada, Y.; Akutsu, Y.; Arai, M.; Tamura, M. *Kayaku Gakkaishi* **2001**, *62*, 147.

(36) da Silva, G.; Bozzelli, J. W. *J. Org. Chem.* **2008**, *73*, 1343.

(37) Ruscic, B.; Wagner, A. F.; Harding, L. B.; Asher, R. L.; Feller, D.; Dixon, D. A.; Peterson, K. A.; Song, Y.; Qian, X.; Ng, C.-Y.; Liu, J.; Chen, W.; Schwenke, D. W. *J. Phys. Chem. A* **2002**, *106*, 2727.

(38) Bystrom, K. *J. Chem. Thermodyn.* **1982**, *14*, 865.

(39) Lin, S.-C.; Kuo, T.-C.; Lee, Y.-P. *J. Chem. Phys.* **1994**, *101*, 2098.

(40) Seta, T.; Nakajima, M.; Miyoshi, A. *Rev. Sci. Instrum.* **2005**, *76*, 064103.

(41) Atkinson, R.; Tuazon, E. C.; Wallington, T. J.; Aschmann, S. M.; Arey, J.; Winer, A. M.; Pitts, J. N., Jr. *Environ. Sci. Technol.* **1987**, *21*, 64.

(42) Prinn, R.; Cunnold, D.; Simmonds, P.; Alyea, F.; Boldi, R.; Crawford, A.; Fraser, P.; Gutzler, D.; Hartley, D.; Rosen, R.; Rasmussen, R. *J. Geophys. Res.* **1992**, *97*, 2445.

(43) Asatryan, R.; Bozzelli, J. W.; Simmie, J. M. *J. Phys. Chem. A* **2008**, *112*, 3172.

JP904156R